Journal of Thermal Analysis and Calorimetry (2021) 144:1083–1093
https://doi.org/10.1007/s10973-020-10488-2

Ceramic properties of kaolinitic clay with monoaluminum phosphate ($Al(H_2PO_4)_3$) addition

A. Mocciaro[1] · M. S. Conconi[1,2] · N. M. Rendtorff[1,2] · A. N. Scian[1,2]

Received: 4 May 2020 / Accepted: 13 December 2020 / Published online: 5 February 2021

Abstract

The effect of monoaluminum phosphate ($Al(H_2PO_4)_3$) addition in the thermochemical process of a kaolinitic clay was studied and compared with the pure clay. Monoaluminum phosphate incorporation is of technological interest for the widely use of this material as an effective binder. From this point of view is important to clarify the processing strategy of kaolinitic clay-MAP based ceramics. This work comprised the characteristics of the obtained ceramics using differential thermal analysis, thermogravimetric analysis (TG), dilatometric analysis, X-ray powder diffraction with Rietveld refinement, mechanical resistance and textural properties. The addition of MAP did not affect the temperature of the kaolinite dehydroxilation (600–500 °C) but reduced this transformation as it was observed in TG curve. The amount of mullite decreased and cristobalite formation was stimulated with MAP presence in the samples fired at 1400 °C. Mullite cell parameters were not modified. The present study gives information for further clay-based materials designed with MAP. It can be concluded that the incorporation of low percentages of MAP in the potential formulation of technological ceramics would not imply important changes in the macroscopic properties of these type of ceramic materials.

Keywords Kaolin · Monoaluminum phosphate · Thermal behavior

Introduction

It is well-known that kaolinitic clays are one of the most widely used clay minerals, being a major component of the raw materials used in the manufacture of ceramics, refractories, cement, filler pigment for paper, cosmetics, etc.

The kaolinitic clays have kaolinite ($Al_2O_3.2SiO_2.2H_2O$) and quartz as major crystalline phases and usually other phases as anatase, rutile, pyrite, siderite, feldspar, etc., depending on the geological conditions under which the kaolinite was formed [1–3].

Kaolinite has a layered 1:1 structure, one layer of the kaolinite consists of an alumina octahedral sheet and a silica tetrahedral sheet that share a common plane of oxygen atoms and repeating layers of the mineral are hydrogen bonded together [4].

The thermal reaction of kaolinite is well known because of its important industrial use [1, 5–9]. Four thermally induced process takes place during calcination of kaolinite: a dehydroxylation of kaolinite to metakaolinite (Eq. 1), then the formation of Al-Si spinel phase from metakaolinite (Eq. 2), after that the formation of mullite (Eq. 3) and, finally, crystallization of cristobalite from amorphous silica (Eq. 4).

$$Al_2O_32SiO_22H_2O \xrightarrow{400-600^{\circ}C} Al_2O_32SiO_2 + H_2O \quad (1)$$

$$2(Al_2O_32SiO_2) \xrightarrow{900-1100^{\circ}C} 2Al_2O_33SiO_2 + SiO_2(\text{amorphus}) \quad (2)$$

$$3(2Al_2O_33SiO_2) \xrightarrow{\geq 1100^{\circ}C} 2(3Al_2O_32SiO_2) + SiO_2(\text{amorphus}) \quad (3)$$

$$SiO_2(\text{amorphus}) \xrightarrow{\geq 1200^{\circ}C} SiO_2(\text{cristobalite}) \quad (4)$$

On the other hand, aluminum phosphate binder ceramic is an inorganic binder used for refractory ceramics and

✉ A. Mocciaro
anamocciaro@cetmic.unlp.edu.ar

[1] CETMIC Centro de Tecnología de Recursos Minerales y Cerámica (CIC-CONICET La Plata), Cno. Centenario y 506, 1897 M.B. Gonnet, Argentina

[2] Departamento de Química. Facultad de Ciencias Exactas, Universidad Nacional de La Plata, Calle 1 y 47., 1900 La Plata, Argentina

coatings to achieve good strength and abrasion resistance [10–13]. Monoaluminum phosphate (MAP or $Al(H_2PO_4)_3$) has been reported as one of the most effective binders because of its high green mechanical strength, high solubility in water, abrasive and corrosive resistance [14]. MAP is proposed as a binder in several systems: refractories castables and mortars [15], corrosion resistance coatings [16], eco-friendly construction material [17], ceramic filters [18], refractories ceramics [19], etc.

According to the literature, MAP can be produced in different ways; one of these is by reaction of phosphoric acid (H_3PO_4) and a reactive alumina (Al_2O_3) source as aluminum hydroxide ($Al(OH)_3$ [20]. In this work, pseudoboehmite ($AlOOH.0.13H_2O$) was used as a reactive alumina source to obtain MAP.

MAP is used as a binder as was mentioned before in different systems especially with clays [19, 21, 22]. Furthermore, kaolinitic clay is used in refractories as a raw material due to its composition of alumina and silica, low cost, good green resistance, etc. In the literature, there is not a systematic analysis of the thermochemical process in the clay-MAP system. This knowledge would be important for future clay-based material designs with the addition of MAP as a binder.

Table 1 Chemical and mineralogical composition of the clay

Oxide	Mass%
Chemical composition Tincar Super clay	
SiO_2	61.82
Al_2O_3	27.55
Fe_2O_3	0.79
MgO	0.66
K_2O	0.76
TiO_2	0.39
CaO	0.28
Na_2O	0.07
Lost of ignition	7.63
Mineralogical composition clay	
Phase	Mass%
Quartz	41
Kaolinite	59

Table 2 Identified crystalline phases, chemical formula and employed PDF card

Crystalline phase	Formula	PDF card
MAP	$Al(H_2PO_4)_3$	00-044-0724
Aluminum tripolyphosphate	$H_2AlP_3O_{10}{\cdot}H_2O$	00-048-0354
Aluminum metaphosphate	$Al(PO_3)_3$	00-013-0430
Aluminum orthophosphate	$Al(PO_4)$	00-011-0500

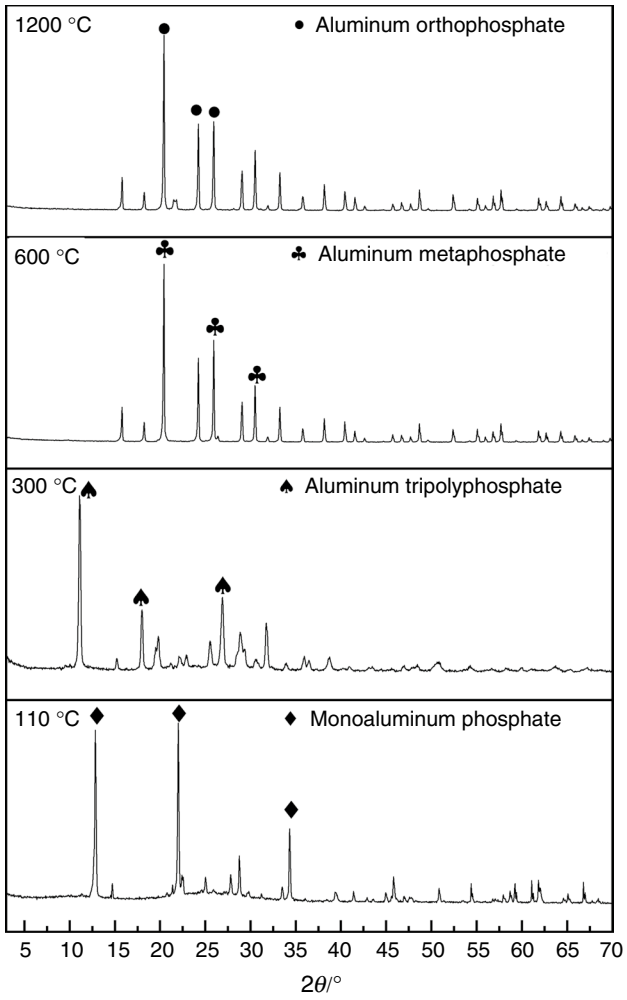

Fig. 1 X-Ray diffraction patterns of MAP fired at 110, 300, 600 and 1200 °C

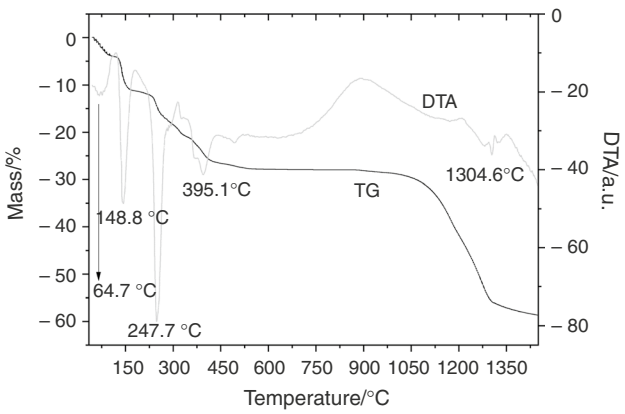

Fig. 2 TG and DTA versus temperature of MAP

The aim of this work is to study and describe the effect of MAP addition in the thermochemical process of a kaolinitic clay and to analyze the changes on the properties of the final

ceramics. The thermochemical characterization of the MAP was also performed to understand its use as additive in kaolinitic clays ceramics.

Experimental

Materials

A commercial clay (Tincar Super Piedra Grande—La Toma Santa Cruz, Argentina [23]) and Monoaluminum phosphate (MAP), made in the laboratory from pseudoboehmite ($AlO(OH)\ 0.13H_2O$) and phosphoric acid (with 95% mass of H_3PO_4) were used for the following research. The chemical and the mineralogical composition of the clay are shown in Table 1.

Processing

Two compositions with 2% and 4% mass of MAP were studied, they were labeled T2M and T4M, respectively, and sample without MAP was labeled T. The mixtures were obtained by mixing the MAP with the kaolinitic clay in a mortar, dried 24 h at 110 °C and then were diagglomerated and sieved (#200) before pressing (Table 2).

Afterward, the mixtures were shaped by uniaxial pressuring into discs (15 mm diameter) and prismatic bars of (50 mm × 7 mm × 7 mm) under a 40 MPa pressure. Prismatic bars were fired in an electric furnace with atmospheric air, with a heating rate of 5 °C min^{-1}, were kept an hour soaking and left to freely cool down. The maximum temperatures reached were 1000, 1100, 1200, 1300 and 1400 °C.

Characterizations

MAP thermal analysis

MAP was evaluated with simultaneous differential thermal (DTA) and thermogravimetric (TG) analysis by a Rigaku Evo Plus II equipment. Both thermal analyses were carried out using 10 °C min^{-1} as heating rate from 25 °C to 1400 °C in air atmosphere. According to the literature [1], the mineralogical composition of the sample at 110, 300, 600 and 1200 °C was confirmed by X-ray diffraction (XRD) technique. XRD analysis was carried out using a Philips PW-3710 diffractometer with Cu Kα (1.5418 Å) radiation, Ni filter at constant voltage 40KV. The XRD patterns were analyzed with the program FullProf (Version 6.0, July 2017).

MAP-clay systems

The behavior of the clay and the clay-MAP mixtures during heating was evaluated by DTA/ TG analysis. A Linseis L74 device was used for the dilatometric analyses, and the temperature range evaluated was from 25 °C to 1350 °C with

Table 3 Compression resistance of T, T2M and T4M before sintering process

	T	T2M	T4M
Compression resistance (MPa)[a]	4.5	5.0	5.5

[a]The standard deviations for mechanical strength: 10%

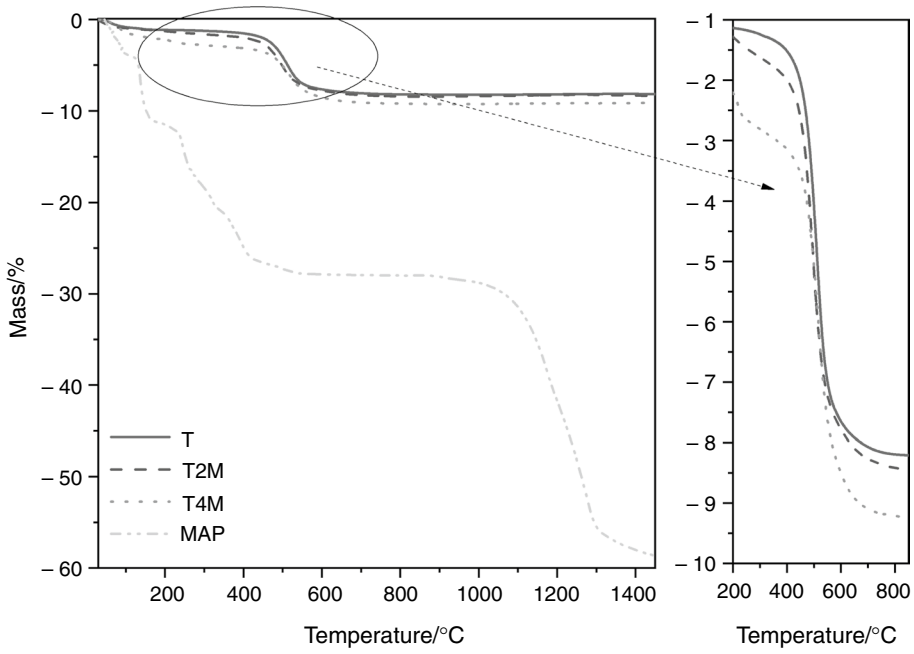

Fig. 3 TG versus temperature of MAP, T, T2M and T4M

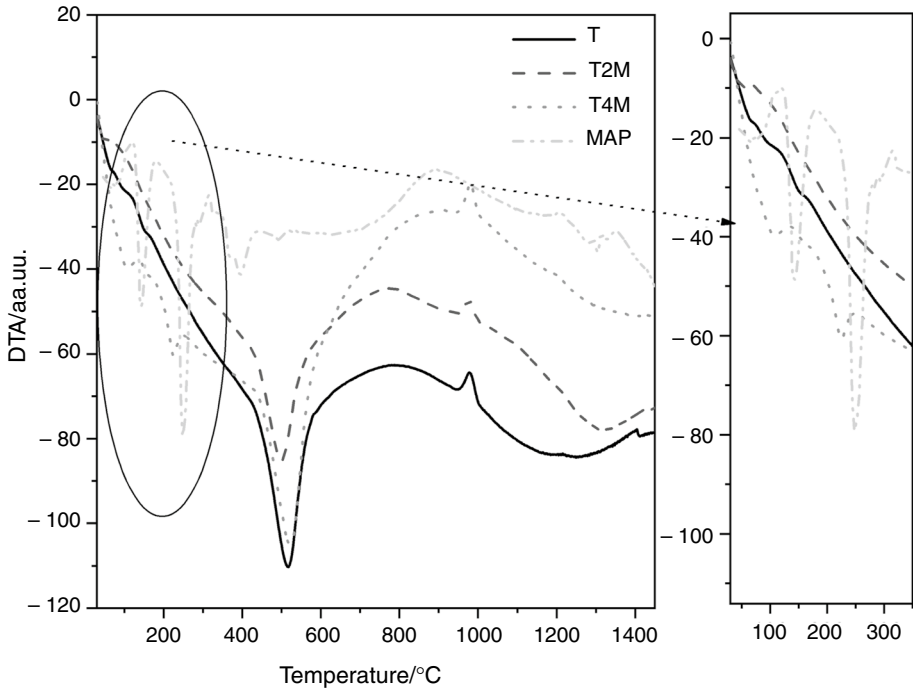

Fig. 4 DTA versus temperature of MAP, T, T2M and T4M

a heating rate of 10 °C min^{-1} in air atmosphere. The crystalline phases of samples sintered at 1000, 1200, 1300, 1400 °C were determined by XRD, and Rietveld method was used for the quantification of the crystalline and amorphous phases [24]. The amorphous phase was quantified by the Le Bail approach, in which this phase is introduced in the refinement as crystalline silica with extremely low crystallite size [25].

The binder effect of MAP in T, T2M and T4M mixtures without thermal treatment was tested by direction compressive strength of pseudo-spherical samples carried out in a universal testing machine (Instron 5985, USA) at a constant strain rate of 0.1 mm min^{-1}, with steel plates.

Finally, mechanical and textural properties of the bars thermal treated at 1000, 1100, 1200, 1300 and 1400 °C were studied. At least five specimens were tested for each test, and an average value was informed. The module of resistance of flexion (MOR) by 3-point bending was evaluated with the same equipment as compressive strength.

The Archimedes' immersion method in water was used to determinate apparent density and open porosity of the fired materials according to ASTM C373-88.

Results and discussions

MAP characterization results

Figure 1 shows the XRD patterns of the MAP after heat treatment at 110, 300, 600, 1200 °C. MAP after heat treatment at 300 °C was in the form of aluminum tripolyphosphate

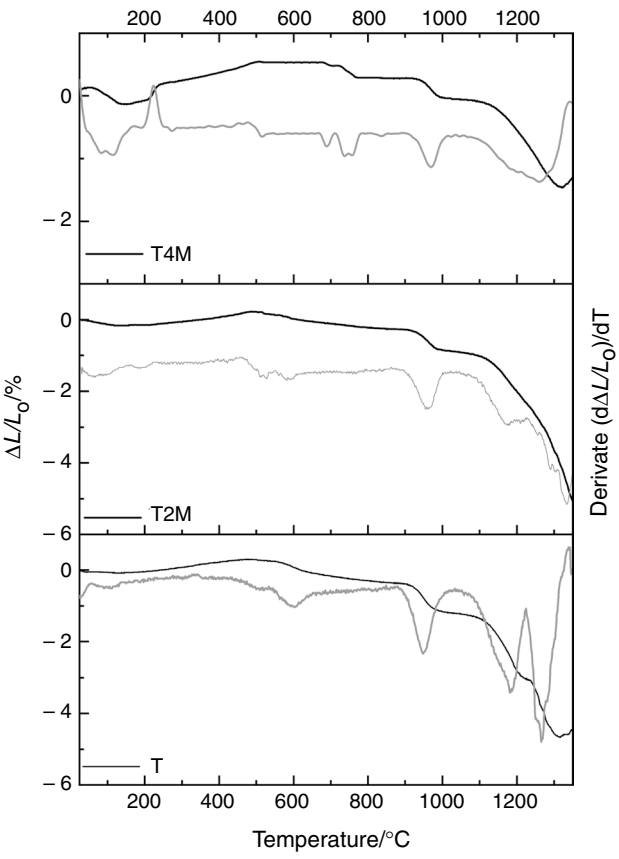

Fig. 5 Dilatometric ($\Delta L.L_o^{-1}$) versus temperature curves and its derivative of T, T2M and T4M mixtures

hydrate ($H_2AlP_3O.10H_2O$) (Eq. 5), because the sample absorbed water due to its high hygroscopicity, this transformation also could be observed in DTA and TG curves (Fig. 2).

In the DTA curve, there is an endothermic band associated with a mass loss (3.8%) which can be observed in the TG curve in the range of 350–450 °C. These changes in the curves are associated with the transformation of tripolyphosphate to aluminum metaphosphate ($Al(PO_3)_3$) with water release (Eq. 6). These crystalline phases were observed in the XRD pattern at 600 °C.

Above 1000 °C, TG curve shows an abrupt decrease (mass loss of 27.4%) and an endothermic peak is observed in the DTA curve. This is caused by the decomposition of aluminum metaphosphate to aluminum orthophosphate ($AlPO_4$) with release of phosphoric oxide (P_2O_5) (Eq. 7).

Based on previous researches [20] and experimental results, the following sequence of thermal transformation was determined for MAP in the temperature range of 110 °C to 1200 °C.

$$Al\left(H_2PO_4\right)_3 \rightarrow H_2AlP_3O_{10} + H_2O \quad (5)$$

$$H_2AlP_3O_{10} \rightarrow Al\left(PO_3\right)_3 + H_2O \quad (6)$$

$$Al\left(PO_3\right)_3 \rightarrow Al\left(PO_4\right) + P_2O_5 \uparrow \quad (7)$$

Effect of MAP as a binder before the sintering process

MAP binding effect in mechanical strength was evaluated by compression tests; Table 3 shows the compressive resistance of the mixtures with the addition of 0, 2 and 4% mass of MAP before sintering. This study shows that additions of MAP slightly enhance the strength of the green samples. This binding effect is higher in grog coarse-grained structural systems [14].

Clay and MAP—clay mixtures thermal analyses

A multitechnique approach was carried out, and Fig. 3 shows TG curves of MAP, T, T2M and T4M. There are differences between MAP curve and clay-MAP curves. The first mass loss of MAP and clay-MAP mixtures is related to dehydration. The mass loss depends on the amount of MAP in the system.

In TG curves of clay-MAP mixtures, between 400 and 800 °C a mass loss is caused by the dehydroxilation of the kaolinite. The mass loss percentages in this temperature range are 6.98, 6.42 and 6.07% for the sample T, T2M and T4M, respectively. This leads to the conclusion that the presence of MAP in the mixture reduces the dehydroxilation of the kaolinite [13].

Above 1000 °C, the abrupt mass loss related to the release of phosphoric oxide (Eq. 7) is only seen on the MAP curve. In clay-MAP mixtures, this mass loss does not appear, so it could be concluded that the phosphoric oxide reaction with spinel and reactive silica present in the system at this temperature (Eq. 2).

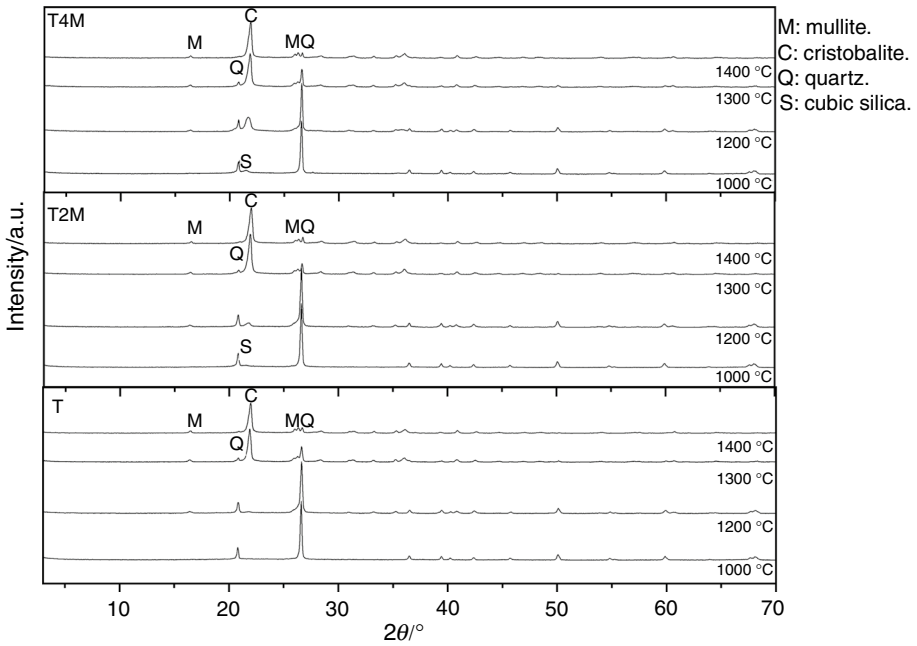

Fig. 6 XRD patterns of the clay and clay-MAP mixtures fired at 1000, 1200, 1300 and 1400 °C

Table 4 Rietveld quantification results of the clay and clay-MAP mixtures fired at 1000, 1200, 1300 and 1400 °C

Sample	T				T2M				T4M			
MAP addition /Mass%	0				2				4			
Firing temperature /°C	1000	1200	1300	1400	1000	1200	1300	1400	1000	1200	1300	1400
Rwp (Residual mass profile)	17.9	15.7	16.0	17.7	15.5	14.2	17.2	17.7	15.9	17.7	17.5	18.5
Quartz	59.0 (20)	49.0 (10)	13.6 (5)	5.7 (6)	62.0 (10)	48.2 (7)	8.9 (6)	5.1 (7)	54.7 (9)	37.0 (10)	14.1 (7)	4.0 (6)
Mullite	–	23.8 (4)	23.6 (3)	25.2 (4)	–	22.3 (3)	18.9 (4)	18.8 (4)	–	13.0 (4)	19.7 (4)	22.5 (4)
Cristobalite 1	–	1.05 (7)	22.1 (4)	24.3 (6)	–	1.7 (1)	12.6 (6)	18.9 (5)	–	24.3 (6)	12.5 (3)	24.3 (6)
Cristobalite 2	–	–	18.5 (3)	21.2 (7)	–	3.5 (2)	39.6 (8)	34.6 (7)	-	7.9 (5)	32.7 (5)	29.7 (6)
Cubic silica	–	–	–	–	1.58 (6)	–	–	–	5.29 (9)	–	–	–
Amorphous phase	41.6 (8)	26.3 (5)	22.3 (3)	23.7 (5)	36.5 (5)	23.3 (3)	20.0 (4)	22.6 (4)	40.0 (5)	17.8 (5)	21.1 (4)	19.6 (4)

Values in parenthesis represent estimated standard deviations in the last quoted place

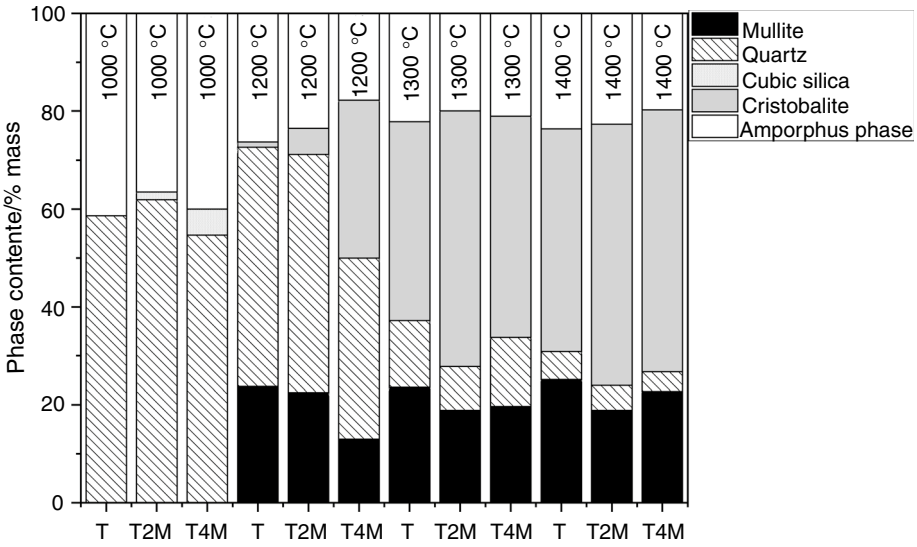

Fig. 7 Crystalline and amorphous phase content as a function of MAP addition fired at 1000, 1200, 1300 and 1400 °C

DTA curves of MAP and of clay with 0, 2 and 4% mass of MAP are showed in Fig. 4. In general, the thermal behavior of clay and clay-MAP mixtures is similar to other kaolinitics clays [5, 26, 27].

MAP's curve presents two endothermic peaks between 100 and 400 °C related with aluminum phosphate transformation. These peaks only appear in the T4M mixture, but these are displaced to lowers temperatures.

Another endothermic peak can be observed in the 400-600ºC range and corresponds to the dehydroxylation of the kaolinite that is overlapped with $\alpha \rightarrow \beta$ quartz transformation with less energy involved [2].

Around 950 °C, one exothermic peak is present in the clay-MAP samples that correspond to metakaolin transformation into the spinel type aluminosilicate phase from primary mullite formation process [1, 5, 28]. MAP addition does not modify temperature range and intensity of exothermic peak associated with the spinel formation process. Finally, second mullite formation after 1100 °C (Eq. 4) was scarcely detected in the studied clay and clay-MAP mixtures.

The dilatometric measurements of the clay and clay-MAP mixtures are showed in Fig. 5, and the studied materials revealed a similar macroscopic thermal behavior in comparison with the ones described in the literature [29, 30]. The first effect observed is a small shrinkage which corresponds to the release of physically adsorbed water, and then thermal expansion range can be observed (positive slope in the TMA), from room temperature to 500 °C. After this temperature, the samples start a minor shrinkage which finishes at around 900 °C followed by an abrupt shrinkage and a clear peak in the $d(\Delta L/L_o)$/dT curve, and this process is associated with the formation of spinel phase (Eq. 2).

After this formation process, a viscous sintering of the clay starts with a shrinkage rate almost constant up to 1320–1370 °C depending on the sample [30]. From this temperature on, mullite formation is observed with a considerably higher expansion achieved for the T2M and T4M samples in comparison with the T sample.

Analysis of crystalline phases after sintering process

XRD patterns of samples fired at different temperatures are shown in Fig. 6. AT 1000 °C, quartz is the major phase in all the mixtures. The samples with MAP addition present a new peak associated with a cubic silica that increases with the amount of MAP in the mixture, according to the literature [31, 32], crystallographic aluminum orthophosphate system is strikingly similar to the silica system. At 1200 °C, the crystalline phases present in all the mixtures are mullite, cristobalite and quartz. The quartz phase decrease and cristobalite phase increase when fired temperature of the samples increases.

Table 4 shows Rietveld quantification of the fired materials. To fit the cristobalite peaks in the Rietveld refinement, two different cristobalite structures were proposed [7, 33, 34]. One form of cristobalite produced by the thermal transformation of quartz present in the clay and the other from the thermal decomposition of kaolinite (they were labeled cristobalite 1 and cristobalite 2, respectively). The first one presenting lower impurities content [7, 26].

In order to understand the effect of MAP addition in the formation of each phase, in Fig. 7 the phase contents (mass % obtained by the Rietveld quantification) are plotted as a function of the MAP % mass added. The stacked bar plot shows that the mullite proportion is slightly over the 20% mass, at 1400 °C, and this proportion decreased with MAP addition. It is well known that this phase defines the mechanical properties of the clay-based ceramic materials.

The amount of mullite at 1400 °C is higher in the T samples than in T2M and T4M samples (25.2%, 18.8% and

Table 5 Cell parameters of the different phases in the materials

Sample	T				T2M				T4M			
Firing temperature /°C	1000	1200	1300	1400	1000	1200	1300	1400	1000	1200	1300	1400
Rwp (Residual mass profile)	17.9	15.7	16.0	17.7	15.5	14.2	17.2	17.7	15.9	17.7	17.5	18.5
Quartz PDF card 01–085-0797												
a (Å)	4.91571	4.91571	4.91571	4.91571	4.91571	4.91571	4.91571	4.91571	4.91571	4.91571	4.91571	4.91571
c (Å)	5.40653	5.40653	5.40653	5.40653	5.40653	5.40653	5.40653	5.40653	5.40653	5.40653	5.40653	5.40653
Mullite PDF card 01–083-1881												
a (Å)	–	7.554 (6)	7.552 (40	7.5468 (3)	–	7.554 (4)	7.556 (4)	7.586 (5)	–	7.557 (8)	7.553 (5)	7.546 (3)
b (Å)	–	7.6941 (6)	7.6993 (4)	7.6947 (4)	–	7.6991 (4)	7.695 (5)	7.6891 (5)	–	7.6995 (8)	7.6988 (5)	7.6969 (4)
c (Å)	–	2.8863 (2)	2.8864 (1)	2.8861 (1)	–	2.8865 (9)	2.8848 (1)	2.8834 (1)	–	2.8838 (2)	2.8861 (1)	2.8837 (4)
Cristobalite 1 PDF card 01–082-0512												
a (Å)		5.020 (20)	4.978 (1)	4.975 (2)	–	4.993 (8)	4.975 (2)	4.970 (2)		5.027 (5)	4.974 (2)	4.979 (2)
c (Å)	–	6.964 (6)	6.9465 (3)	6.9323 (3)	–	6.980 (2)	6.9344 (5)	6.9176 (4)	–	6.963 (1)	6.9321 (5)	6.9462 (4)
Cristobalite 2 PDF card 01–082-0512												
a (Å)	–	–	5.006 (3)	5.004 (3)	–	5.030 (10)	4.995 (3)	4.995 (2)	–	4.989 (6)	4.999 (3)	5.010 (3)
c (Å)	–	–	7.005 (20)	6.9919 (7)	–	7.040 (30)	6.9790 (6)	6.9704 (5)	-	7.040 (1)	6.9820 (6)	6.9974 (7)
Cubic silica PDF card 01–089-3435												
a (Å)	–	–	–	–	7.140 (10)	–	–	–	–	7.135 (6)	–	–

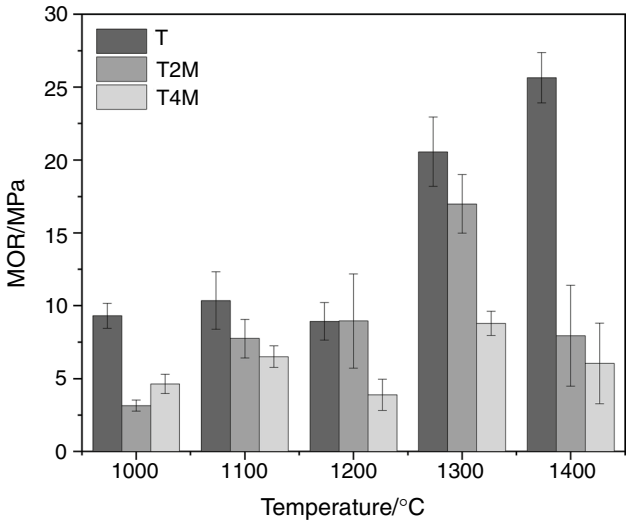

Fig. 8 The module of resistance of flexion (MOR) of T, T2M and T4M samples as a function of the fired temperature

22.5%, respectively). The quartz proportion after 1400 °C is around 4–6% for all the mixtures, but the total cristobalite proportion is 45.4%, 53.5% and 54% for T, T2M and T4M, respectively. This shows that the MAP addition stimulates cristobalite formation and decreases the percentage of amorphous phase, probably due to the lower viscosity of the resulting transient amorphous phase at high temperature [35].

The cristobalite produced by the thermal decomposition of kaolinite (cristobalite 2) at 1300 and 1400 °C is present in major percentage in T2M and T4M samples. Possibly, there are impurities and/or defects in this cristobalite phase due formation mechanism that cannot be detected in these techniques.

The refined cell parameters and the Rwp parameters are shown in Table 5, the Rwp value is a parameter used for assessing the quality for qualify of the Rietveld refinement, and the obtained values are acceptable and similar to others found in the literature for similar materials [36]. The mullite cell parameters are in accordance with the literature [37], and it can be observed that MAP addition does not modify mullite structure.

Mechanical and textural properties after the sintering process

Figure 8 shows module of resistance of flexion (MOR) values of MAP-clay mixtures fired at different temperatures. The results indicate that MOR values increase with increasing firing temperature, and the flexural strength of the materials is influenced by their phase composition. The increase in refractory phases (cristobalite and mullite) and the densification of the materials improved their flexural strength. It was observed that at any sintering temperature, clay without MAP has higher MOR values compared to clay-MAP mixtures. At 1400 °C, the MOR values are 26.0, 8.0 and 6.0 MPa for T, T2M and T4M, respectively; this is mostly related to the percentage of mullite crystalline phase which gives it greater mechanical resistance to ceramics.

The apparent density and open porosity of the fired samples (Fig. 9) show the effect of the studied additive. In all formulations, the density of the material increases at a higher temperature, while the porosity decreases; this increment of the density is related to the elimination of the pores and the sintering of the materials [33]. The achieved density values are in accordance with the ones expected [2], T samples having density values between 1.76 and 2.03 $g.cm^{-3}$. MAP addition in the mixtures does not produce major changes

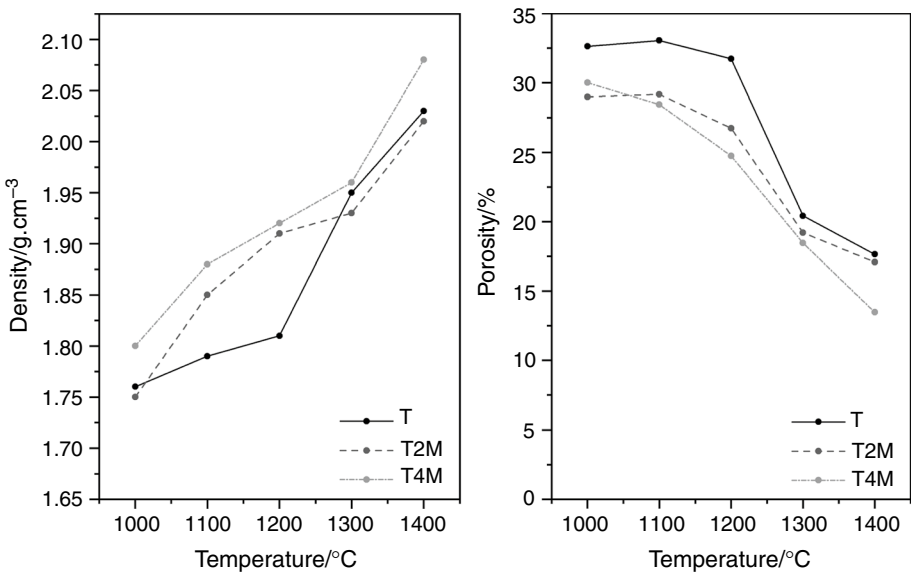

Fig. 9 Apparent density (g cm^{-3}) and open porosity (%) of T, T2M and T4M samples as a function of the temperature

of apparent density values, but it decreases the open porosity percentage reached. T samples fired at 1400 have 17.6% porosity, while T4M samples with the same thermal process have 13.5% porosity. According to the crystallographic analysis, it can be concluded that the porosity effect observed in Fig. 9 is only textural and it is not related to mineralogical changes.

Conclusions

The effect of MAP addition in the thermochemical process of a kaolinitic clay and the characterization of the final ceramics fired at 1000, 1100, 1200, 1300 and 1400 °C was performed. MAP is of technological interest because of its use as a binder in coatings, refractories ceramics, refractories castables and mortars, eco-friendly construction material, etc. From this point of view, it is important to clarify the processing strategy of kaolinitic clay-MAP-based ceramics.

The addition of MAP did not interfere in the temperature of the kaolinite dehydroxilation (500–600 °C) but decreased the mass loss as seen in the TG curve, in this range of temperature. This enables to conclude that the presence of MAP in the mixture reduced the dehydroxilation of the kaolinite. Furthermore, the spinel temperature formation and the shrinkage associated with this process were modified by the presence of MAP in the formulation.

X-ray diffraction and Rietveld refinement corroborate the evolution of crystalline and amorphous phases. Like the model clay, mixtures fired at 1400 °C had mullite and cristobalite as principal phases accompanied by quartz and amorphous phase. The only aluminum containing crystalline phase is mullite ($3Al_2O_3.2SiO_2$), all the resulting crystalline phases contain silicon (mullite, residual not reacted quartz (SiO_2) and cristobalites (SiO_2—quartz derived and crystallized)). As no other P containing phase was detected by XRD, presumably the phosphorus oxide is present in the complex triplex SiO_2-Al_2O_3-P_2O_5 non-crystalline phase. The amount of mullite slightly decreased, this might be explained by the dilution effect accompanied by an increase in the glassy phase content due to the incorporation of P to the formulation. Cristobalite formation was enhanced with MAP presence in the formulation. Mullite cell parameters were not affected; therefore, MAP did not modify mullite structure.

MAP addition did not affect significantly the open porosity and apparent density of the fired ceramics. However, the 4% mass, addition at 1400 °C decreased flexural strength; this was related to the mullite phase percentage, which gives it greater mechanical resistance in ceramics.

Finally, it can be concluded that the incorporation of low percentages of MAP in the potential formulation of technological ceramics would not imply important changes in the macroscopic properties of these type of ceramic materials.

Acknowledgements This work was supported by CONICET. This work has been partially supported by Nano-Petro FONARSEC Project 2012 (ANPCyT). N.M.R. thanks FONCyT-BID PICT 2016-1193.

References

1. Chakraborty AK. Phase transformation of kaolinite clay. New Delhi: Springer; 2014.
2. Dondi M, Raimondo M, Zanelli C. Clays and bodies for ceramic tiles: reappraisal and technological classification. Appl Clay Sci. 2014;96:91–109.
3. Schroeder PA, Erickson G. Kaolin: from ancient porcelains to nanocomposites. Elements. 2014;10:177–82.
4. Konta J. Clay and man: clay raw materials in the service of man. Appl Clay Sci. 1995;10:275–335.
5. Andrini L, Gauna MR, Conconi MS, Suarez G, Requejo G, Aglietti EF, et al. Extended and local structural description of a kaolinitic clay, its fired ceramics and intermediates: an XRD and XANES analysis. Appl Clay Sci. 2016;124–125:39–45.
6. Torres Sánchez RM, Basaldella EI, Marco JF. The effect of thermal and mechanical treatments on kaolinite: characterization by XPS and IEP measurements. J Colloid Interface Sci. 1999;215:339–44.
7. Hernández MF, Violini MA, Serra MF, et al. Boric acid (H_3BO_3) as flux agent of clay-based ceramics, B_2O_3 effect in clay thermal behavior and resultant ceramics properties. J Therm Anal Calorim. 2020;139:1717–29.
8. Ondruška J, Csáki Š, Štubňa I, et al. Investigation of kaolin–quartz mixtures during heating using thermodilatometry and DC thermoconductometry. J Therm Anal Calorim. 2020;139:833–8.
9. Al-Shantir O, Csáki Š, Ondro T, et al. Mechanical-acoustic study of electroporcelain mixture made under different compression pressures. J Therm Anal Calorim. 2020;142(5):1759–66.
10. Chen D, He L, Shang S. Study on aluminum phosphate binder and related Al_2O_3–SiC ceramic coating. Mater Sci Eng. 2003;348:29–35.
11. Kingery WD. Fundamental study of phosphate bonding in refractories: I, literature review. J Am Ceram Soc. 1950;33:239–41.
12. Vippola M, et al. Structural characterization of aluminum phosphate binder. J Am Ceram Soc. 2000;83:1834–6.
13. Sahnoun RD, Bouaziz J. Sintering characteristics of kaolin in the presence of phosphoric acid binder. Ceram Int. 2012;38:1–7.
14. Luz AP, Gomes DT, Pandolfelli VC. High-alumina phosphate-bonded refractory castables: $Al(OH)_3$ sources and their effects. Ceram Int. 2015;41:9041–50.
15. Hipedinger NE, Scian AN, Aglietti EF. Magnesia-phosphate bond for cold-setting cordierite-based refractories. Cem Concr Res. 2002;32:675–82.
16. Colonetti E, Hobold Kammer E, De Noni JA. Chemically-bonded phosphate ceramics obtained from aluminum anodizing waste for use as coatings. Ceram Int. 2014;40:14431–8.
17. Wang YS, Dai JG, Ding Z, Xu mass% Phosphate-based geopolymer: formation mechanism and thermal stability. Mater Lett. 2017;190:209–12.
18. Almanza RJM, Castillejos EAH, Acosta GFA, Flores VA. Microstructure and properties characterization of a new ceramic filter —CEFILPB. Mater Des. 1994;15:135–40.
19. Mocciaro A, Lombardi MB, Scian AN. Effect of raw material milling on ceramic proppants properties. Appl Clay Sci. 2018;153:90–4.
20. Morris JH, Perkins PG, Rose AEA, Smith WE. The chemistry and binding properties of aluminium phosphates. Chem Soc Rev. 1977;6:173–94.

21. Almanza RJM, Castillejos EAH, Acosta GFA, Flores VA. Microstructure and properties characterization of a new ceramic filter CEFILPB. Mater Des. 1994;15:135–40.
22. Zulkifly K, et al. 2020 Thermal exposure of fly ash-metakaolin blend geopolymer with addition of monoaluminum phosphate (MAP). In: IOP Conf. Ser.: Mater. Sci. Eng. https://doi.org/10.1088/1757-899X/864/1/012011.
23. Dominguez E, Cravero F. Los recursos de caolín de Chubut y Santa Cruz. Recur Miner Repub Argent. Zappettini E.O. Argentina: Instituto de Geología y Recursos Minerales. Secretaría de Estado de Geología y Minería de Argentina; 1999. pp. 1265–1272.
24. Rietveld HM. A profile refinement method for nuclear and magnetic structures. J Appl Crystallogr. 1969;2:65–71.
25. Le Bail A. Modelling the silica glass structure by the Rietveld method. J Non Cryst Solids. 1995;183:39–42.
26. Hernández MF, Conconi MS, Cipollone M, Herrera MS, Rendtorff NM. Ceramic behavior of ball clay with gadolinium oxide (Gd_2O_3) addition. Appl Clay Sci. 2017;146:380–7.
27. Xu X, et al. Microstructural evolution, phase transformation, and variations in physical properties of coal series kaolin powder compact during firing. Appl Clay Sci. 2015;115:76–86.
28. Okada K, Otsuka N, Ossaka J. Characterization of spinel phase formed in the kaolin-mullite thermal sequence. J Am Ceram Soc. 1986;69:C251–3.
29. Ptáček P, et al. The kinetics and mechanism of kaolin powder sintering I. The dilatometric CRH study of sinter-crystallization of mullite and cristobalite. Powder Technol. 2012;232:24–30.
30. Zanelli C, Raimondo M, Guarini G, Dondi M. The vitreous phase of porcelain stoneware: composition, evolution during sintering and physical properties. J Non Cryst Solids. 2011;357:3251–60.
31. Beck WR. Crystallographic inversions of the aluminum orthophosphate polymorphs and their relation to those of silica. J Am Ceram Soc. 1949;32:147–51.
32. Kumar P, Tiwari AN, Bhargava P. Effect of process parameters and binder concentration on mechanical properties of phosphate bonded alumina. Trans Indian Ceram Soc. 2013;72:130–5.
33. Butler MA, Dyson DJ. The quantification of different forms of cristobalite in devitrified alumino-silicate ceramic fibres. J Appl Crystallogr. 1997;30:467–75.
34. Madsen IC, Finney RJ, Flann RCA, Frost MT, Wilson BW. Quantitative analysis of high-alumina refractories using X-ray powder diffraction data and the rietveld method. J Am Ceram Soc. 1991;74:619–24.
35. Karlsson KH, Rönnlöf M. Property-composition relationships for potentially bioactive glasses. Glass Sci Technol (Frankfurt). 1998;71(5):141–5.
36. Herrera MS, Hernández MF, Cipollone M, Conconi MS, Rendtorff NM. Thermal behavior of samarium oxide—Ball clay mixtures for high macroscopic neutron capture cross section ceramic materials. Appl Clay Sci. 2019;168:125–35.
37. Schneider H, Schreuer J, Hildmann B. Structure and properties of mullite—a review. J Eur Ceram Soc. 2008;28:329–44.